Robust Receiver Design for High Altitude Aircraft Navigation with Terrestrial Cellular Signals

Zaher M. Kassas
The Ohio State University
Columbus, OH, USA
zkassas@ieee.org

Shaghayegh Shahcheraghi
The Ohio State University
Columbus, OH, USA
shahcheraghi.1@osu.edu

Ali Kaiss
The Ohio State University
Columbus, OH, USA
kaiss.1@osu.edu

Chiawei Lee
United States Air Force
Edwards Air Force Base, CA, USA

Juan Jurado
United States Air Force
Edwards Air Force Base, CA, USA

Steven Wachtel
United States Air Force
Edwards Air Force Base, CA, USA

Jacob Duede
United States Air Force
Edwards Air Force Base, CA, USA

Zachary Hoeffner
United States Air Force
Edwards Air Force Base, CA, USA

Thomas Hulsey
United States Air Force
Edwards Air Force Base, CA, USA

Rachel Quirarte
United States Air Force
Edwards Air Force Base, CA, USA

RunXuan Tay
Republic of Singapore Air Force
Singapore, Republic of Singapore

***Abstract*—A robust receiver design to exploit long-term evolution (LTE) terrestrial cellular signals of opportunity (SOPs) for high altitude aircraft navigation is presented. Conventional receivers employ phase-locked loops (PLLs) to track the carrier phase of received signals. In this paper, a Kalman filter (KF) is developed to replace the receiver's PLLs. To evaluate the performance of the proposed receiver, a flight campaign was conducted over two regions in California, USA: (i) Region A: Edwards Air Force Base (rural) and (ii) Region B: Palmdale (semi-urban). It is shown that the proposed receiver provides robust tracking of received LTE signals compared to a conventional PLL-based receiver, in which the latter could only track intermittently, especially during sharp turns. The produced carrier phase observables to 5 LTE eNodeBs in each region were fused with altimeter data via an extended Kalman filter (EKF) to estimate the aircraft's trajectory. Over trajectories of 51 km and 57 km in regions A and B, traversed in 9 min and 11 min, at flying altitudes of 5,000 and 7,000 ft above ground level, respectively, the proposed KF-based receiver reduced the position root-mean squared error (RMSE) by 74.8% and 30.7%, respectively, over the PLL-based receiver.**

***Index Terms*—Aircraft navigation, signals of opportunity, LTE**

I. Introduction

Radio frequency interference (RFI) incidents in global navigation satellite system (GNSS) bands have skyrocketed in the past few years, jeopardizing safe and efficient aviation operations [1]. National agencies, from the U.S. Department of Transportation (USDOT) [2] to the National Institute of Standards and Technology (NIST) [3], and international agencies, from the International Civil Aviation Organization (ICAO) [4], [5] to the International Telecommunication Union (ITU) [6], have called for both protecting against harmful RFI in GNSS bands and to finding complementary navigation technologies. In its highly regarded 2021 report, NIST identified signals of opportunity (SOPs) and terrestrial RF sources (e.g., cellular) as a mitigation category.

SOPs have demonstrated promising potential for navigation when GNSS signals become unreliable or unavailable [7]. Even though these signals were not intended for navigation purposes, researchers have shown that they can be exploited for such purpose. SOPs can be terrestrial (e.g., AM/FM radio [8]–[10], cellular [11]–[13], and digital television [14]–[16]), or space-based (e.g., low Earth orbit (LEO) satellites [17]–[19] and geostationary Earth orbit (GEO) satellites [20]).

Cellular SOPs have been shown to be particularly effective as a navigation source in challenging GNSS environments, such as indoors [21], [22], deep urban canyons [23], [24], and intentionally GPS-jammed environments [25]. This is attributed to their inherent features, which are desirable for navigation: abundance, geometrical and spectral diversity, and reception with a high carrier-to-noise ratio (CNR). When it comes to aerial vehicle navigation, cellular signals have yielded submeter-level accuracy on low altitude unmanned aerial vehicles (UAVs) [26], [27] and meter-level accuracy on high altitude aircraft [28]–[30].

Assessing cellular signals for aerial vehicles have been the subject of several studies recently [31], [32]. These studies span radio channel modeling [33], [34]; evaluation of signal quality in terms of received signal power [35], [36], interference from cellular transmitters [37], [38], and coverage and connectivity [39], [40]; and standards recommendations

[41], [42]. However, the majority of these studies focused on evaluating cellular signals for communication purposes with little attention to evaluating them for navigation purposes [43], [44]. Moreover, they considered UAVs flying at low altitudes (up to 500 ft) and slow speeds (up to 50 km/h).

To the authors knowledge, the first studies to evaluate the potential of cellular signals for high altitude aircraft navigation appeared in [28]–[30]. These studies were the result of an unprecedented aerial campaign conducted by the Autonomous Systems Perception, Intelligence, and Navigation (ASPIN) Laboratory in collaboration with the United States Air Force (USAF) at the Edwards Air Force Base (AFB), California, USA. The cellular software-defined radios (SDRs) of the ASPIN Laboratory were flown on a USAF Beechcraft C-12 Huron, a fixed-wing aircraft, to collect ambient cellular signals. This unique dataset consists of combinations of flights run over rural and semi-urban environments with altitudes ranging up to 23,000 ft and a multitude of trajectories and maneuvers including straight segments, banking turns, holding patterns, and ascending and descending teardrops, performed by members of the USAF Test Pilot School.

Conventional receivers [45], including the one used in [28]–[30], employ phase-locked loops (PLLs) to track the carrier phase of received signals. Kalman filter (KF)-based tracking loops are known to improve tracking robustness [46], [47], which are adopted in this paper. The proposed KF-based receiver was evaluated on recorded long-term evolution (LTE) samples over two regions in California, USA: (i) Region A: Edwards Air Force Base (rural) and (ii) Region B: Palmdale (semi-urban). This paper shows that the KF-based receiver provides robust tracking compared to a conventional PLL-based receiver, in which the latter could only track intermittently, especially during sharp turns. The produced carrier phase observables to 5 LTE eNodeBs in each region were fused with altimeter data via an extended Kalman filter (EKF) to estimate the aircraft's trajectory. Over trajectories of 51 km and 57 km in regions A and B, traversed in 9 min and 11 min, at flying altitudes of 5,000 and 7,000 ft above ground level (AGL), respectively, the proposed KF-based receiver reduced the position root-mean squared error (RMSE) by 74.8% and 30.7%, respectively, over the PLL-based receiver.

The rest of this article is organized as follows. Section II describes the proposed KF-based tracking loops. Section III evaluates the tracking performance of the proposed receiver. Section IV describes the EKF settings and compares the aircraft navigation results obtained using the PLL-based receiver versus the proposed KF-based receiver. Section V gives concluding remarks.

II. Proposed KF-Based Tracking Loops

This section outlines the proposed KF-based tracking loops, which are later shown to improve carrier phase tracking robustness over PLL-based tracking. Aside from the tracking loops, the remainder of the receiver components remain identical to the receiver used in [28]–[30].

A. KF-based Tracking Design

In [28], it was shown that during aircraft banking, tracking was lost, which resulted in large navigation error. One reason for the tracking loss was that the PLL could not cope with such high dynamics. To address this issue, the PLL is replaced with a KF to track the carrier phase, Doppler, and Doppler rate.

1) Received Signal Dynamical Model: Using a Taylor series expansion, the carrier phase of the received signal can be represented as

$$\theta = \theta_0 + \dot{\theta}(t)t + \frac{1}{2}\ddot{\theta}(t)t^2 + \cdots. \tag{1}$$

In this paper, the carrier phase is approximated up to its second-order term to provide robust tracking by estimating both the Doppler frequency and Doppler rate. The state vector is defined as $\boldsymbol{x}(t) = [\theta(t), \dot{\theta}(t), \ddot{\theta}(t)]$, whose dynamics is modeled as

$$\begin{aligned} \dot{\boldsymbol{x}}(t) &= \mathbf{A}\boldsymbol{x}(t) + \mathbf{B}\tilde{\boldsymbol{w}}(t) \\ \mathbf{A} = \begin{bmatrix} 0 & 1 & 0 \\ 0 & 0 & 1 \\ 0 & 0 & 0 \end{bmatrix}, &\quad \mathbf{B} = \begin{bmatrix} 0 \\ 0 \\ 1 \end{bmatrix}, \end{aligned} \tag{2}$$

where $\tilde{\boldsymbol{w}}(t)$ is a zero-mean white noise process with power spectral density $q_{\tilde{w}}$. The continuous-time model in (2) is discretized at a time interval, known as subaccumulation interval, T_{sub}, yielding

$$\boldsymbol{x}_{k+1} = \mathbf{F}\boldsymbol{x}_k + \boldsymbol{w}_k, \tag{3}$$

where $\mathbf{F} = e^{\mathbf{A}T_{sub}}$; $T_{sub} = LT_s$, where T_s is the baseband sampling time, and L is the number of samples in each T_{sub}; $\boldsymbol{w}_k$ is a discrete-time process noise vector, which is a zero-mean white sequence with covariance $\mathbf{Q} = q_{\tilde{w}} \int_0^{T_{sub}} e^{\mathbf{A}T_{sub}} (e^{\mathbf{A}T_{sub}})^{\mathsf{T}} dt$.

B. Kalman Filter-Based Tracking Loop

In the proposed receiver, a third-order KF-based algorithm is designed to track the carrier phase, Doppler frequency, and Doppler rate. Denote $\hat{\boldsymbol{\theta}}_{k|k}$ as the estimate of the state vector at time-step k, given all the measurements up to time-step k. The estimate of the state vector is $\hat{\boldsymbol{\theta}} = [\hat{\theta}_0, 2\pi\hat{f}_D, 2\pi\dot{\hat{f}}_D]$. The initial state vector estimate is $\hat{\boldsymbol{\theta}}_{0|0} = [0, 2\pi f_{D_0}, 0]$, where f_{D_0} is estimated from the acquisition step. The estimated carrier phase $\hat{\theta} = \hat{\theta}_0 + 2\pi\hat{f}_D n T_s + 2\pi\frac{\dot{\hat{f}}_D}{2} n^2 T_s^2$ is used for both Doppler and Doppler rate wipe-off according to $\tilde{\boldsymbol{r}}[n] = \boldsymbol{r}[n]\exp(-j\hat{\theta})$, where $\boldsymbol{r}[n]$ is the received baseband signal, which can be expressed as

$$\begin{aligned} r[n] = \alpha c[\tau_n - t_s[n]]\exp(j\theta[\tau_n]) \\ + d[\tau_n - t_s[n]]\exp(j\theta[\tau_n]) + w[n], \end{aligned} \tag{4}$$

where α is the complex channel gain between the receiver and the eNodeB, τ_n is the sample time expressed in the receiver time, $c[n]$ is the periodic reference signal (namely, the secondary synchronization signal (SSS) and cell-specific reference signal (CRS), in this paper), $t_s[n]$ is the code phase

related to the distance between the receiver and the eNodeB at the nth time instant, $\theta[\tau_n]$ is the carrier phase in radians, $d[\tau_n]$ represents the data samples transmitted from the eNodeB, and $w[n]$ the measurement noise, modeled as an independent and identically distributed white noise.

Equivalently, the received signal can be represented as

$$r[n] = s[n] + w_{equ}[n], \tag{5}$$

where the desired received signal can be represented as

$$s[n] = \alpha c[\tau_n - t_s[n]] \exp(j\theta[\tau_n]) \tag{6}$$

and the equivalent noise is

$$w_{equ}[n] = d[\tau_n - t_s[n]] \exp(j\theta[\tau_n]) + w[n]. \tag{7}$$

After compensating for the carrier phase, the received signal can be written as

$$r[n] = \alpha c[\tau_n - t_s[n]] \exp(j\tilde{\theta}[\tau_n]) + n_k[n], \tag{8}$$

where $\tilde{\theta}_k[n] = \theta_k[n] - \hat{\theta}_k[n]$ is the carrier phase estimation error. The wiped-off sequence is correlated with the locally generated code. The angle of this correlation is considered as the residual error and is fed as an innovation to the KF loop using the observation model

$$\boldsymbol{z}_k = \mathbf{H}\boldsymbol{x}_k + \boldsymbol{v}_k, \quad \mathbf{H} = \begin{bmatrix} 1 & 0 & 0 \end{bmatrix}, \tag{9}$$

where $\boldsymbol{v}_k$ is the observation noise, which is modeled as discrete-time zero-mean white sequence with variance σ_θ^2. After calculating the innovation and performing a measurement-update step, the posterior carrier phase state $\hat{\boldsymbol{\theta}}_{k|k}$ is estimated and used in the refinement of the tracking.

C. Carrier-Aided Delay-Locked Loop

The carrier-aided delay-locked loop (DLL) uses a dot-product discriminator [48] to calculate the code phase error using the prompt, early, and late correlations, represented by S_p, S_e, and S_l. The early and late correlations are computed by correlating the received signal with an early and delayed version of the prompt code sequence, respectively to yield

$$e_k = C \cdot \left[(I_{e,k} - I_{l,k}) I_{p,k} + (Q_{e,k} - Q_{l,k}) Q_{p,k} \right], \tag{10}$$

where $S_{p,k} = I_{p,k} + jQ_{p,k}$, $S_{e,k} = I_{e,k} + jQ_{e,k}$, and $S_{l,k} = I_{l,k} + jQ_{l,k}$ and the constant C relates to the CNR and chip interval. The DLL loop filter is a simple gain K, which relates to the noise-equivalent bandwidth, $B_{n,DLL} = \frac{K}{4} = 0.05$. The output of the DLL filter, $\nu_{DLL,k}$, is the rate of change of the code phase, expressed in $\frac{\text{s}}{\text{s}}$. Assuming low-side mixing, the code start time is updated at time intervals of T_{sub} according to

$$\hat{t}_{s_{k+1}} = \hat{t}_{s_k} - (\nu_{DLL,k} + \frac{\hat{f}_{Dk}}{f_c}) T_{sub}, \tag{11}$$

where f_c is the carrier frequency, $\hat{f}_{Dk}$ is the Doppler frequency estimated by the KF, and T_{sub} is the subaccumulation interval.

III. Tracking Results

To evaluate the performance of the proposed receiver, the same LTE samples used in [28]–[30] was re-processed. The tracking results from proposed receiver versus [30] are compared in this section.

A. Region A

The first test trajectory is shown in Fig. 1. During this flight, data was sampled from two LTE channels with carrier frequencies at (i) 731.5 MHz, a 4G LTE channel allocated for the US cellular provider T-Mobile, and (ii) 751 MHz, a 4G LTE channel allocated for the US cellular provider AT&T. The robustness of the proposed receiver is evaluated by comparing its performance for the five eNodeBs that were acquired and tracked in [30]. Fig. 2a illustrates the time history of the pseudoranges obtained from carrier phase measurements that were estimated using the proposed KF-based receiver versus the ground truth ranges for the five LTE eNodeBs. Fig. 2b shows the time history of the measured pseudoranges estimated in [30] versus the ground truth ranges for those five LTE eNodeBs. The results demonstrate that pseudorange tracking is lost only for one eNodeB (around 350 s), while in [30], tracking was lost for three eNodeBs, starting around 300 s, the time at which the aircraft performed a banking turn.

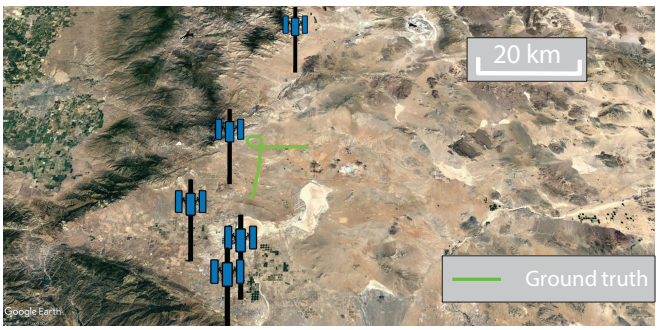

Fig. 1: Experimental environment in region A showing the aircraft trajectory and the locations of the 5 LTE eNodeBs.

B. Region B

The second test trajectory is shown in Fig. 3. During this flight, two LTE channels were sampled at (i) 731.5 MHz, a 4G LTE channel allocated for T-Mobile, and (ii) 739 MHz, a 4G LTE channel allocated for Verizon. In [30], five LTE eNodeBs were acquired and tracked during this flight. Fig. 4a illustrates the time history of the pseudoranges estimated using the proposed KF-based receiver versus the ground truth ranges for the five LTE eNodeBs. Fig. 4b shows the time history of the measured pseudoranges estimated in [30] versus the ground truth ranges for those five LTE eNodeBs. It can be seen that the KF-based receiver tracks more eNodeBs for longer time compared with [30].

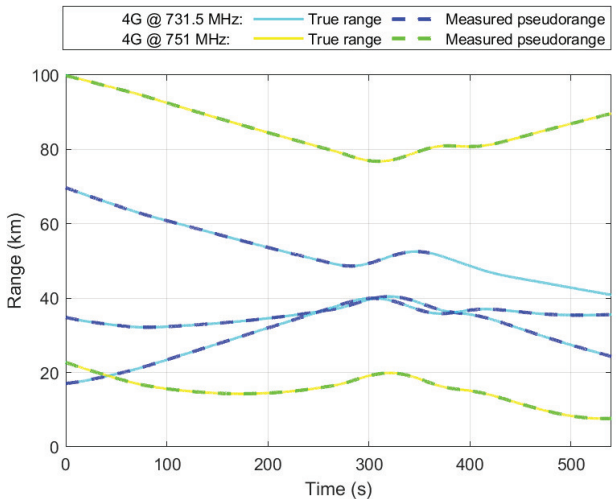

(a)

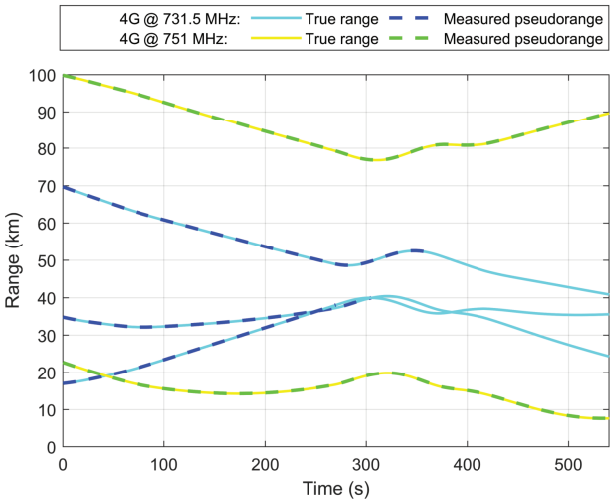

(b)

Fig. 2: Time history of the pseudoranges and the corresponding true range in Region A using (a) the proposed KF-based receiver and (b) the PLL-based received used in [30]. The initial values of the pseudoranges were subtracted out for ease of comparison.

C. Discussion

The results presented in Subsections III-A and III-B highlight the robustness of the proposed KF-based tracking loop compared to PLL-based tracking. Using a third-order KF enabled tracking more eNodeBs for a longer period of time. This improved performance is due to the fact that using a third-order KF, the Doppler rate is also tracked. In addition, in each iteration, the carrier phase error is used to update the measurement variance, which affects Doppler estimation, and improves the tracking. It is worth noting that the loss of tracking in the proposed KF-based receiver could be attributed to the blockage caused by the wings or the body of the aircraft,

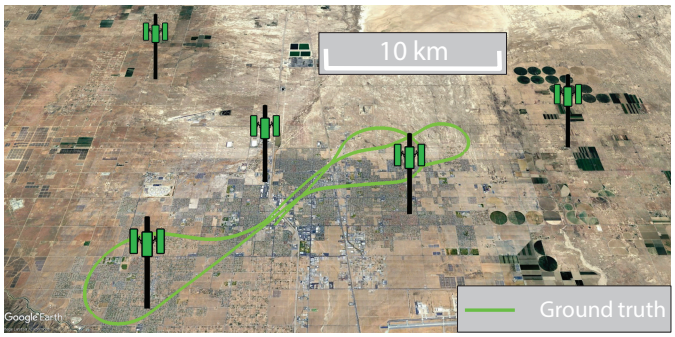

Fig. 3: Experimental environment in region A showing the aircraft trajectory and the locations of the 5 LTE eNodeBs.

which attenuate the signal. It could be also attributed to the KF failing to keep up with highly dynamic aircraft maneuvers. Investigation of this phenomenon is deferred to future research.

IV. Navigation Results

The produced carrier phase observables to five LTE eNodeBs in each region were fused with altimeter data via an EKF to estimate the aircraft's trajectory. The EKF used in this paper is similar to the one adopted in [30]. The EKF settings are summarized next.

The receiver and nth LTE eNodeB clock process noise covariance matrices were set to

$$c^2\mathbf{Q}_{clk_r} = \begin{bmatrix} 4.22 \times 10^{-5} & 3.37 \times 10^{-7} \\ 3.37 \times 10^{-7} & 6.74 \times 10^{-5} \end{bmatrix}$$

$$c^2\mathbf{Q}_{clk_{sn}} = \begin{bmatrix} 3.59 \times 10^{-5} & 3.54 \times 10^{-9} \\ 3.54 \times 10^{-9} & 7.09 \times 10^{-7} \end{bmatrix},$$

where c is the speed of light and $n = 1, 2, \ldots, 5$. The measurement sampling time was $T = 0.01$ s. The jerk process noise spectra were chosen to $\tilde{q}_N = \tilde{q}_E = 15\,\mathrm{m}^2/\mathrm{s}^5$ and $\tilde{q}_D = 5\,\mathrm{m}^2/\mathrm{s}^5$. The altimeter measurement noise variance $\sigma^2_{alt}(k)$ was set to $5\,\mathrm{m}^2$. The measurement noise variance was calculated from the CNR.

The navigation performance of the proposed receiver is compared with PLL-based receiver in Table II and Table III for both regions. Over trajectories of 51 km and 57 km in regions A and B, traversed in 9 min and 11 min, at flying altitudes of 5,000 and 7,000 ft AGL, respectively, the proposed KF-based receiver reduced the position RMSE by 74.8% and 30.7%, respectively, over the PLL-based receiver. The PLL-based receiver in [30] lost track of several eNodeBs during the banking turns. It is worth noting that the results presented in [30] included signals received from cellular 3G code-division multiple access (CDMA), which yielded a meter-level accurate navigation solution. These CDMA signals are omitted in this papers to focus on assessing the performance of only LTE signals. It is expected that adding the omitted CDMA pseudoranges into the EKF would yield meter-level accurate navigation which would be more accurate than the results reported in [30].

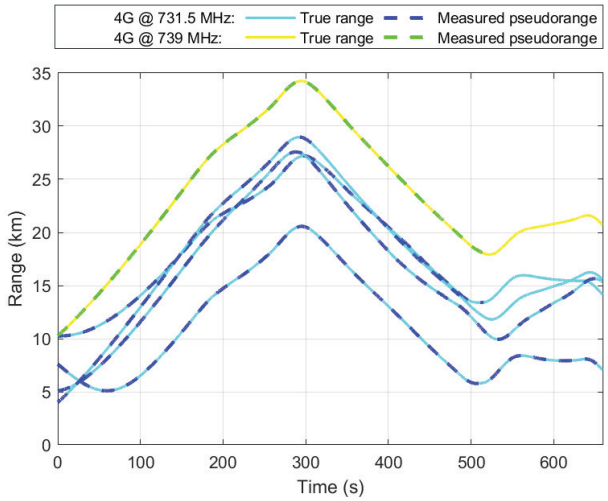

(a)

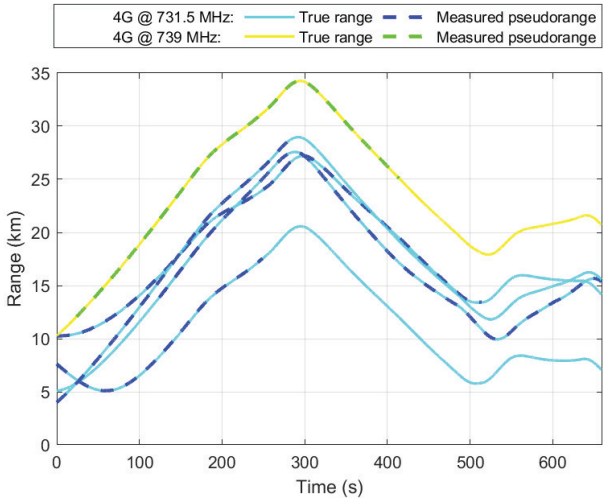

(b)

Fig. 4: Time history of the pseudoranges and the corresponding true range in Region B using (a) the proposed KF-based receiver and (b) the PLL-based received used in [30]. The initial values of the pseudoranges were subtracted out for ease of comparison.

V. Conclusion

This paper presented a KF-based receiver design to track the carrier phase of terrestrial cellular LTE signals on high altitude aircraft. Re-processing the dataset recorded in the SNIFFER flight campaign with the proposed KF-based receiver was shown to produce robust tracking compared with a PLL-based receiver. In addition, the produced carrier phase observables were fused with altimeter data via an EKF to estimate the aircraft's trajectory. Over trajectories of 51 km and 57 km in regions A and B, traversed in 9 min and 11 min, at altitude of 5,000 ft and 7,000 ft AGL, respectively, the proposed KF-based receiver reduced the position RMSE by 74.8% and 30.7%, respectively, over the PLL-based receiver.

TABLE I: Navigation Performance in Region A

Metric	PLL	Proposed KF
Number of eNodeBs used	5	5
Cellular Frequency [MHz]	731.5	731.5
	751	751
Flight duration [min]	9	9
Flight length [km]	44	44
Altitude AGL [ft]	5,000	5,000
Position RMSE [m]	119.25	30.03
Position error standard deviation [m]	88.51	20.79

TABLE II: Navigation Performance in Region B

Metric	PLL	Proposed KF
Number of eNodeBs used	5	5
Cellular Frequency [MHz]	731.5	731.5
	739	739
Flight duration [min]	11	11
Flight length [km]	57	57
Altitude AGL [ft]	7,000	7,000
Position RMSE [m]	211.33	146.44
Position error standard deviation [m]	183.11	113.25

Acknowledgment

This work was supported in part by the Air Force Office of Scientific Research (AFOSR) under Grant FA9550-22-1-0476 and in part by the U.S. Department of Transportation (USDOT) under Grant 69A3552047138 for the CARMEN University Transportation Center (UTC). The authors would like to thank Edwards AFB and Holloman AFB for inviting the ASPIN Laboratory to conduct experiments on USAF aircraft in the "SNIFFER: Signals of opportunity for Navigation In Frequency-Forbidden EnviRonments" flight campaign. The authors would like to thank Joshua Morales, Kimia Shamaei, Mahdi Maaref, Kyle Semelka, MyLinh Nguyen, and Trier Mortlock for their help with preparing for data collection and Joe Khalife and Ali Abdallah for their help with data processing. DISTRIBUTION STATEMENT A. Approved for public release; Distribution is unlimited. 412TW-PA-20146.

References

[1] EUROCONTROL, Aviation Intelligence Unit, "Does radio frequency interference to satellite navigation pose an increasing threat to network efficiency, cost-effectiveness and ultimately safety?," tech. rep., March 2021.

[2] A. Hansen, S. Mackey, H. Wassaf, E. Wallischeck, C. Scarpone, M. Barzach, and E. Baskerville, "Complementary PNT and GPS backup technologies demonstration report: Sections 1 through 10," *John A. Volpe National Transportation Systems Center (US)*, no. DOT-VNTSC-20-07, 2021.

[3] M. Bartock, J. Brule, Y. Li-Baboud, S. Lightman, J. McCarthy, K. Reczek, D. Northrip, A. Scholz, and T. Suloway, "Foundational PNT profile: Applying the cybersecurity framework for the responsible use of positioning, navigation, and timing (PNT) services," *National Institute of Standards and Technology (NIST)*, February 2021.

[4] International Civil Aviation Organization (ICAO), "An urgent need to address harmful interferences to GNSS," tech. rep., May 2019.

[5] International Civil Aviation Organization (ICAO), "Strengthening of communications, navigation, and surveillance (CNS) systems resilience and mitigation of interference to global navigation satellite system (GNSS)," tech. rep., 2020.

[6] International Telecommunication Union , "Prevention of harmful interference to radio navigation satellite service receivers in the 1559 – 1610 mhz frequency band," tech. rep., July 2022.

[7] J. Raquet *et al.*, "Position, navigation, and timing technologies in the 21st century," vol. 2, Part D: Position, Navigation, and Timing Using Radio Signals-of-Opportunity, ch. 35–43, pp. 1115–1412, Wiley-IEEE, 2021.

[8] J. McEllroy, J. Raquet, and M. Temple, "Use of a software radio to evaluate signals of opportunity for navigation," in *Proceedings of ION GNSS Conference*, pp. 126–133, September 2006.

[9] X. Chen, Q. Wei, F. Wang, Z. Jun, S. Wu, and A. Men, "Super-resolution time of arrival estimation for a symbiotic FM radio data system," *IEEE Transactions on Broadcasting*, vol. 66, pp. 847–856, December 2020.

[10] M. Psiaki and B. Slosman, "Tracking digital FM OFDM signals for the determination of navigation observables," *NAVIGATION, Journal of the Institute of Navigation*, vol. 69, no. 2, 2022.

[11] A. Abdallah, J. Khalife, and Z. Kassas, "Exploiting on-demand 5G downlink signals for opportunistic navigation," *IEEE Signal Processing Letters*, vol. 30, pp. 389–393, 2023.

[12] J. Tian, L. Fangchi, T. Yafei, and L. Dongmei, "Utilization of non-coherent accumulation for LTE TOA estimation in weak los signal environments," *EURASIP Journal on Wireless Communications and Networking*, vol. 2023, no. 1, pp. 1–31, 2023.

[13] S. Morgan and S. Martin, "Performance analysis of a cellular LTE and GPS L1 C/A vector tracking receiver, a simulation study," in *Proceedings of ION International Technical Meeting*, pp. 692–707, January 2023.

[14] N. Souli, P. Kolios, and G. Ellinas, "Relative positioning of autonomous systems using signals of opportunity," in *Proceedings of IEEE Vehicular Technology Conference*, pp. 1–6, 2020.

[15] T. Hong, J. Sun, T. Jin, Y. Yi, and J. Qu, "Hybrid positioning with DTMB and LTE signals," in *Proceedings of International Wireless Communications and Mobile Computing*, pp. 303–307, July 2021.

[16] Z. Jiao, L. Chen, X. Lu, Z. Liu, X. Zhou, Y. Zhuang, and G. Guo, "Carrier phase ranging with DTMB signals for urban pedestrian localization and GNSS aiding," *Remote Sensing*, vol. 15, no. 2, pp. 423–446, 2023.

[17] C. Pinell, "Receiver architectures for positioning with low Earth orbit satellite signals," Master's thesis, Lulea University of Technology, School of Electrical Engineering, Sweden, 2021.

[18] C. Zhao, H. Qin, N. Wu, and D. Wang, "Analysis of baseline impact on differential doppler positioning and performance improvement method for LEO opportunistic navigation," *IEEE Transactions on Instrumentation and Measurement*, pp. 1–10, 2023.

[19] Z. Kassas, N. Khairallah, and S. Kozhaya, "Ad astra: Simultaneous tracking and navigation with megaconstellation LEO satellites," *IEEE Aerospace and Electronic Systems Magazine*, 2023. accepted.

[20] Y. Gao, X. Zhao, S. Wang, Y. Xiang, C. Huang, and Y. Hua, "Positioning via GEO communication satellites' signals of opportunity," *IET Radar, Sonar Navigation*, vol. 15, pp. 1472–1482, July 2021.

[21] A. Abdallah and Z. Kassas, "Multipath mitigation via synthetic aperture beamforming for indoor and deep urban navigation," *IEEE Transactions on Vehicular Technology*, vol. 70, pp. 8838–8853, September 2021.

[22] C. Jao, A. Abdallah, C. Chen, M. Seo, S. Kia, Z. Kassas, and A. Shkel, "PINDOC: Pedestrian indoor navigation system integrating deterministic, opportunistic, and cooperative functionalities," *IEEE Sensors Journal*, vol. 22, pp. 14424–14435, July 2022.

[23] Z. Kassas, M. Maaref, J. Morales, J. Khalife, and K. Shamaei, "Robust vehicular localization and map matching in urban environments through IMU, GNSS, and cellular signals," *IEEE Intelligent Transportation Systems Magazine*, vol. 12, pp. 36–52, June 2020.

[24] R. Whiton, J. Chen, T. Johansson, and F. Tufvesson, "Urban navigation with LTE using a large antenna array and machine learning," in *Proceedings of IEEE Vehicular Technology Conference*, pp. 1–5, 2022.

[25] Z. Kassas, J. Khalife, A. Abdallah, and C. Lee, "I am not afraid of the GPS jammer: resilient navigation via signals of opportunity in GPS-denied environments," *IEEE Aerospace and Electronic Systems Magazine*, vol. 37, pp. 4–19, July 2022.

[26] J. Khalife and Z. Kassas, "On the achievability of submeter-accurate UAV navigation with cellular signals exploiting loose network synchronization," *IEEE Transactions on Aerospace and Electronic Systems*, vol. 58, pp. 4261–4278, October 2022.

[27] J. Khalife and Z. Kassas, "Differential framework for submeter-accurate vehicular navigation with cellular signals," *IEEE Transactions on Intelligent Vehicles*, vol. 8, pp. 732–744, January 2023.

[28] Z. Kassas, J. Khalife, A. Abdallah, C. Lee, J. Jurado, S. Wachtel, J. Duede, Z. Hoeffner, T. Hulsey, R. Quirarte, and R. Tay, "Assessment of cellular signals of opportunity for high-altitude aircraft navigation," *IEEE Aerospace and Electronic Systems Magazine*, vol. 37, pp. 4–19, October 2022.

[29] Z. Kassas, A. Abdallah, J. Khalife, C. Lee, J. Jurado, J. Duede, Z. Hoeffner, T. Hulsey, R. Quirarte, S. Wachtel, and R. Tay, "Received power characterization of terrestrial cellular signals on high altitude aircraft," in *Proceedings of IEEE Aerospace Conference*, pp. 1–8, March 2022.

[30] Z. Kassas, J. Khalife, A. Abdallah, C. Lee, J. Jurado, J. Duede, Z. Hoeffner, T. Hulsey, R. Quirarte, S. Wachtel, and R. Tay, "Flight demonstration of high altitude aircraft navigation with cellular signals," *IEEE Intelligent Transportation Systems Magazine*. accepted.

[31] Qualcomm Technologies, Inc., "LTE unmanned aircraft systems," Tech. Rep. 1.0.1, May 2017.

[32] Y. Zeng, Q. Wu, and R. Zhang, "Accessing from the sky: A tutorial on UAV communications for 5G and beyond," *Proceedings of the IEEE*, vol. 107, pp. 2327–2375, December 2019.

[33] X. Cai, J. Rodriguez-Pineiro, X. Yin, N. Wang, B. Ai, G. Pedersen, and A. Yuste, "An empirical air-to-ground channel model based on passive measurements in LTE," *IEEE Transactions on Vehicular Technology*, vol. 68, pp. 1140–1154, February 2019.

[34] W. Khawaja, I. Guvenc, D. Matolak, U. Fiebig, and N. Schneckenburger, "A survey of air-to-ground propagation channel modeling for unmanned aerial vehicles," *IEEE Communications Surveys & Tutorials*, vol. 21, no. 3, pp. 2361–2391, 2019.

[35] K. Matheou, R. Apaza, A. Downey, R. Kerczewski, J. Jung, C. Ippolito, and H. Modi, "Analysis of at-altitude LTE power spectra for small unmanned aircraft system C2 communications," in *Proceedings of Integrated Communications, Navigation and Surveillance Conference*, pp. 1–12, April 2019.

[36] X. Cai, N. Wang, J. Rodriguez-Pineiro, X. Yin, A. Yuste, W. Fan, G. Zhang, G. Pedersen, and L. Tian, "Low altitude air-to-ground channel characterization in LTE network," in *Proceedings of European Conference on Antennas and Propagation*, pp. 1–5, April 2019.

[37] I. Kovacs, R. Amorim, H. Nguyen, J. Wigard, and P. Mogensen, "Interference analysis for UAV connectivity over LTE using aerial radio measurements," in *Proceedings of IEEE Vehicular Technology Conference*, pp. 1–6, September 2017.

[38] R. Amorim, J. Wigard, I. Kovacs, and T. Sorensen, "UAV communications for 5G and beyond," ch. 5: Performance Enhancements for LTE-Connected UAVs: Experiments and Simulations, pp. 139–161, Wiley-IEEE, 2021.

[39] E. Teng, J. Diogo Falcao, and B. Iannucci, "Holes-in-the-sky: A field study on cellular-connected UAS," in *Proceedings of International Conference on Unmanned Aircraft Systems*, pp. 1165–1174, June 2017.

[40] B. Stevens and M. Younis, "Detection algorithm for cellular synchronization signals in airborne applications," *IEEE Access*, vol. 9, pp. 55555–55566, April 2021.

[41] A. Abdalla and V. Marojevic, "Communications standards for unmanned aircraft systems: The 3GPP perspective and research drivers," *IEEE Communications Standards Magazine*, vol. 5, pp. 70–77, March 2021.

[42] H. Maattanen, "UAV communications for 5G and beyond," ch. 6: 3GPP Standardization for Cellular-Supported UAVs, pp. 163–180, Wiley-IEEE, 2021.

[43] E. Kim and Y. Shin, "Feasibility analysis of LTE-based UAS navigation in deep urban areas and DSRC augmentation," *Sensors*, vol. 19, pp. 4192–4207, April 2019.

[44] J. Mortier, G. Pages, and J. Vila-Valls, "Robust TOA-based UAS navigation under model mismatch in GNSS-denied harsh environments," *Remote Sensing*, vol. 12, pp. 2928–2947, September 2020.

[45] M. Braasch and A. Dempster, "Tutorial: GPS receiver architectures, front-end and baseband signal processing," *IEEE Aerospace and Electronic Systems Magazine*, vol. 34, no. 2, pp. 20–37, 2019.

[46] J. Won, T. Pany, and B. Eissfeller, "Characteristics of Kalman filters for GNSS signal tracking loop," *IEEE Transactions on Aerospace and Electronic Systems*, vol. 48, pp. 3671–3681, October 2012.

[47] J. Vila-Valls, P. Closas, M. Navarro, and C. Fernandez-Prades, "Are PLLs dead? a tutorial on Kalman filter-based techniques for digital carrier synchronization," *IEEE Aerospace and Electronic Systems Magazine*, vol. 32, no. 7, pp. 28–45, 2017.

[48] A. van Dierendonck, P. Fenton, and T. Ford, "Theory and performance of narrow correlator spacing in a GPS receiver," *NAVIGATION, Journal of the Institute of Navigation*, vol. 39, pp. 265–283, September 1992.